

# Network inference from oscillatory signals based on circle map

Akari Matsuki\*

*Faculty of Advanced Life Science, Hokkaido University, Sapporo 060-0810, Japan*

Hiroshi Kori†

*Graduate School of Frontier Sciences, The University of Tokyo, Chiba 277-8561, Japan*

Ryota Kobayashi‡

*Graduate School of Frontier Sciences, The University of Tokyo, Chiba 277-8561, Japan  
Mathematics and Informatics Center, The University of Tokyo, Tokyo, 113-8656, Japan*

(Dated: September 4, 2024)

Synchronization is ubiquitous in nature, which is mathematically described by coupled oscillators. Synchronization strongly depends on the interaction network, and the network plays a crucial role in controlling the dynamics. To understand and control synchronization dynamics in the real world, it is essential to identify the network from the observed data. While previous studies have developed the methods for inferring the network of asynchronous systems, it remains challenging to infer the network of well-synchronized oscillators. In this study, we develop a method for non-invasively inferring the network of synchronized and desynchronized oscillators. This method is based on the circle map, which describes the phase change in an oscillatory cycle. Our method discards a large part of data used for inference, which may seem counterintuitive. However, the effectiveness of the method is supported by the phase reduction theory, a well-established theory for analyzing weakly coupled oscillators. We verify the proposed method by applying it to simulated data of the limit-cycle oscillators. This study provides an important step towards understanding synchronization in real-world systems from a network perspective.

## I. INTRODUCTION

Synchronization is an emergent phenomenon in a population of dynamically interacting units, which plays an important role in a range of systems, including physical, biological, chemical, engineering, and social systems [1]. Synchronization phenomena are mathematically described by coupled oscillators, where an individual oscillator is modeled as a limit-cycle oscillator [2, 3]. Phase reduction theory [3–6] is a powerful framework for analyzing the synchronization of the coupled oscillators. This theory provides a unified mathematical description of the dynamics of coupled oscillators by representing the state of the oscillator using a single variable of the phase and describing their dynamics using a reduced phase model. Theoretical studies based on the phase model have elucidated the key components underlying synchronization phenomena [1, 3, 5, 7].

Synchronization of coupled oscillators depends strongly on the interaction network, which describes how the oscillators interact with each other. The structure [8–10] as well as the weight [11, 12] of the network influence the synchronizability of the oscillators (see reviews [13, 14]). Furthermore, the network can even qualitatively change the synchronization properties. For the majority of networks, the Kuramoto model exhibits continuous synchronization transitions: the system starts to synchronize when the interaction strength reaches a threshold. However, the threshold is dramatically decreased in the presence of hub nodes and even vanishes in scale-free networks [15, 16]. It is also known that when the structural and the dynamical properties are correlated, the synchronization transition becomes discontinuous (also known as “explosive synchronization”) [17, 18]. Moreover, the network plays a central role in controlling the synchronization dynamics. For example, the control of abnormal synchronization is closely related to the treatment of brain disorders such as Parkinson’s disease [19, 20]. From the network structure, it is possible to evaluate the controllability, that is, which oscillators should be stimulated to control the system to any desired state [21, 22].

To understand and control synchronization dynamics in the real world, it is essential to identify the interaction network. While it is becoming possible to measure the dynamics of individual oscillators in the network, it is often difficult to directly measure the network. Consequently, it is necessary to infer the network from the observed oscillatory signals [23–25]. For desynchronized systems, various methods of network inference have been developed

---

\* akarimatsuki@sci.hokudai.ac.jp

† kori@k.u-tokyo.ac.jp

‡ r-koba@k.u-tokyo.ac.jp

[24–34]. On the contrary, it is still challenging to infer the network of well-synchronized systems, where the oscillators are nearly phase-locked [26, 29, 35]. A common methodology for inferring the network of synchronous systems is to disrupt synchronization by external perturbations. However, this approach requires the implementation of experimental interventions in human and animal subjects, which can present technical and ethical challenges. A more fundamental problem is that the invasion can deteriorate the properties of the system. Therefore, it is preferable to infer the network from non-invasively measured data.

In this study, we propose a method for inferring the network from non-invasively measured oscillatory data with high accuracy regardless of synchrony or asynchrony. A common approach is to fit the data to a set of differential equations that describe the dynamics of the phase oscillators and infer the model parameters, including the network. However, this approach is inadequate for inferring the network due to the difficulties that arise when using short-time phase changes. To address these problems, we develop an inference method based on the circle map, which describes the phase change over a period of the oscillator. The proposed method discards a large part of the data used for inference, which may seem counterintuitive. However, the effectiveness of the method is supported by the phase reduction theory. Furthermore, our method is applicable to a variety of oscillatory systems, since the circle map is derived from a general system of weakly coupled oscillators. To test the validity of the proposed method, we apply it to simulated data from two realistic limit-cycle oscillator models: the Brusselator for chemical oscillators and the model of circadian oscillators in the suprachiasmatic nucleus (SCN).

This paper is organized as follows. In Sec. II, we describe the phase description of coupled oscillators. In Sec. III, we introduce a naive method for network inference and discuss its issues. In Sec. IV, we present our proposed method and demonstrate that it performs better than the naive method. We apply the proposed method to simulated data from the Brusselator model and the model of circadian oscillators in the SCN. Finally, we conclude this paper and discuss future directions.

## II. PHASE DESCRIPTION OF COUPLED OSCILLATORS

We present a theory for the phase description of coupled oscillators. Details can be found in the literature [3–5]. We first consider a limit-cycle oscillator whose dynamics are given by

$$\frac{d\mathbf{X}}{dt} = \mathbf{F}(\mathbf{X}), \quad (1)$$

where  $t$  is time,  $\mathbf{X} \in \mathbb{R}^d$  represents the oscillator state,  $\mathbf{F}(\mathbf{X}) \in \mathbb{R}^d$  describes the oscillator dynamics. Suppose this dynamical system (1) has the limit-cycle. Let  $\mathbf{X}_0(t)$ ,  $T$ , and  $\omega = 2\pi/T$  be the orbit, the period of the limit-cycle, i.e.,  $\mathbf{X}_0(t+T) = \mathbf{X}_0(t)$ , and the natural frequency, respectively. For a state  $\mathbf{X}$  in the basin of attraction of the limit-cycle, we can define the scalar field  $\Phi_{\mathbf{F}}(\mathbf{X}) : \mathbb{R}^d \rightarrow \mathbb{R}$ , referred to as the phase function, such that the phase  $\phi(t) = \Phi_{\mathbf{F}}(\mathbf{X}(t))$  satisfies

$$\frac{d\phi}{dt} = \omega. \quad (2)$$

Here we focus on a system of  $N$  weakly coupled limit-cycle oscillators. The dynamics of oscillator  $i$  ( $i = 1, \dots, N$ ) can be written as

$$\frac{d\mathbf{X}_i}{dt} = \mathbf{F}(\mathbf{X}_i) + \epsilon \mathbf{f}_i(\mathbf{X}_i) + \epsilon \sum_{j=1}^N \mathbf{Q}_{ij}(\mathbf{X}_i, \mathbf{X}_j) + \boldsymbol{\eta}_i(t), \quad (3)$$

where  $\epsilon$  is a small dimensionless parameter that characterizes the degree of heterogeneity and the coupling strength (i.e., the interaction strength),  $\epsilon \mathbf{f}_i(\mathbf{X}_i)$  represents the difference of the intrinsic dynamics of oscillator  $i$  from  $\mathbf{F}(\mathbf{X}_i)$ , and  $\epsilon \mathbf{Q}_{ij}(\mathbf{X}_i, \mathbf{X}_j)$  represents the interaction from oscillator  $j$  to oscillator  $i$ . The noise term  $\boldsymbol{\eta}_i(t)$  is assumed to be the Gaussian white noise obeying  $E[\boldsymbol{\eta}_i(t)] = \mathbf{0}$  and  $\text{Cov}[\boldsymbol{\eta}_i(t)\boldsymbol{\eta}_i(s)] = v_i^2 I_d \delta(t-s)$ , where  $I_d$  is the identity matrix of size  $d$ ,  $v_i^2$  is the noise variance, and  $\delta(t)$  is the Dirac's delta function. In the following, we further assume that the noise variance  $v_i^2$  is sufficiently smaller than  $\epsilon$  and neglect terms of  $O(v_i^2)$  [36, 37]. All other quantities including  $\mathbf{F}$ ,  $\mathbf{G}$ ,  $v_i$  are  $O(1)$ . Next, we consider the dynamics of the phase of oscillator  $i$ ,  $\phi_i = \Phi_{\mathbf{F}}(\mathbf{X}_i)$ . The dynamics of the phase  $\phi_i(t)$  deviates from Eq. (2) by  $O(\epsilon)$ . Specifically, by neglecting  $O(\epsilon^2)$  and  $O(v_i^2)$  terms, we obtain

$$\frac{d\phi_i}{dt} = \omega + \epsilon \nu_i(\phi_i) + \epsilon \sum_{j=1}^N q_{ij}(\phi_i, \phi_j) + \mathbf{Z}(\phi_i) \cdot \boldsymbol{\eta}_i(t), \quad (4)$$

where  $\mathbf{Z}(\phi) := \text{grad}_{\mathbf{X}} \Phi|_{\mathbf{X}=\mathbf{X}_0(\phi/\omega)}$  is the phase sensitivity function. The derivation of Eq. (4) is given in Appendix A. Thus, the  $dN$ -dimensional dynamical system, given by Eq. (3), is reduced to the  $N$ -dimensional system. Moreover, by applying the averaging approximation to Eq. (4), we can derive a simpler equation

$$\frac{d\phi_i}{dt} = \omega_i + \sum_{j=1}^N c_{ij} \gamma_{ij}(\phi_j - \phi_i) + \sigma_i \xi_i(t), \quad (5)$$

where

$$\omega_i = \omega + \frac{\epsilon}{2\pi} \int_0^{2\pi} \nu_i(\phi) d\phi, \quad (6)$$

$$c_{ij} = \frac{\epsilon}{\sqrt{\pi}} \left\| \frac{1}{2\pi} \int_0^{2\pi} q_{ij}(\psi, \psi + \phi) d\psi \right\|, \quad (7)$$

$$\gamma_{ij}(\phi) = \sqrt{\pi} \frac{\int_0^{2\pi} q_{ij}(\psi, \psi + \phi) d\psi}{\left\| \int_0^{2\pi} q_{ij}(\psi, \psi + \phi) d\psi \right\|}, \quad (\text{if } c_{ij} \neq 0) \quad (8)$$

$$\sigma_i^2 = \frac{v_i^2}{2\pi} \int_0^{2\pi} \mathbf{Z}^T(\phi) \mathbf{Z}(\phi) d\phi, \quad (9)$$

are the natural frequency of oscillator  $i$ , the coupling strength from oscillator  $j$  to  $i$ , the averaged coupling function, and the noise variance, respectively,  $\xi_i(t)$  is the Gaussian white noise with the mean 0 and the variance 1, and

$\|f(\phi)\| := \left( \int_0^{2\pi} (f(\phi))^2 d\phi \right)^{1/2}$  is the  $L_2$  norm of the function  $f(\phi)$ .

We should note the difference between the phase of the non-averaged equation (4) and the phase of the averaged equation (5). To avoid confusion, we write  $\phi_i$  and  $\phi_j$  in the averaged equation (5) as  $\varphi_i$  and  $\varphi_j$ , respectively. Neglecting the noise term, the averaging approximation can be obtained from a variable transformation, so called the near-identity transformation:

$$\varphi_i = \phi_i + \epsilon h_i(\phi_1, \dots, \phi_N). \quad (10)$$

where  $h_i$  is a  $2\pi$ -periodic function of  $O(1)$  [3, 5, 38, 39]. Eq.(10) implies that these phases are actually different by  $O(\epsilon)$ . This discrepancy leads to a critical degradation of the inference method proposed in Sec. III.

### III. NAIVE METHOD FOR INFERRING THE OSCILLATOR NETWORK

Our goal is to infer the interaction network or coupling network, i.e. the coupling strengths among oscillators, from the oscillatory signals. As illustrated in Fig. 1, we first reconstruct the phase  $\phi_i(t)$  of each oscillator from the observation  $y_i(t)$  and fit the reconstructed phases to a model. Thanks to the phase reduction theory (see Sec. II), our approach via phase reconstruction is generally applicable to arbitrary limit-cycle oscillators with weak heterogeneity, coupling, and noise. Moreover, it is not necessary to infer the detailed properties of the oscillators, since we are only interested in identifying the interaction network. Therefore, it makes sense to consider a phase oscillator model as a model for inferring the network. There are two types of phase oscillator models: the non-averaged and the averaged models, given as Eq. (4) and Eq. (5), respectively. The former model approximates the oscillatory dynamics more accurately, whereas the latter has a simpler description while keeping the information of the interaction network. Thus, we use the averaged model (5) for inferring the underlying network from the reconstructed phase.

It is challenging to infer the interaction network from the observed data when the oscillators are partially synchronized or in a nearly phase-locked state [26, 29, 35]. To reduce the difficulty, we make two assumptions for the network inference. First, we assume that the coupling function is the same for all the pairs,  $\gamma_{ij}(\phi_j - \phi_i) = \gamma(\phi_j - \phi_i)$ . This assumption is valid for a wide variety of systems, including some systems of cardiac cells [40] and neurons [7, 41, 42]. Second, we assume that the sinusoidal function for the averaged coupling function [43]. This assumption is reasonable when the oscillation is close to the Hopf bifurcation [3, 44]. Furthermore, it would be impossible to infer the coupling function including higher harmonic terms when the oscillators are nearly phase-locked, because the inference requires the information on the dynamics for various phase differences. Therefore, we assume

$$\gamma_{ij}(\phi_j - \phi_i) = \sin(\phi_j - \phi_i + \alpha), \quad (11)$$

where  $\alpha$  is a parameter that controls the stable phase-locked state. Substituting Eq. (11) into Eq. (5) and discretizing it, we obtain a model that is used for the inference of our first method:

$$\delta\phi_{i,k} = h \left\{ \omega_i + \sum_{j=1}^N c_{ij} \sin(\phi_{j,k} - \phi_{i,k} + \alpha) \right\} + \sqrt{h}\sigma_i\xi_{i,k}, \quad (12)$$

where  $\phi_{i,k} := \phi_i(kh)$ ,  $\delta\phi_{i,k} := \phi_{i,k+1} - \phi_{i,k}$  is the phase change in the sampling interval  $h$ , and  $\xi_{i,k}$  is the independent gaussian random variable with mean 0 and variance 1. Finally, we can obtain the network  $\{c_{ij}\}$  by fitting the reconstructed phase  $\{\phi_{i,k}\}$  to Eq. (12) using maximum likelihood method. Note that we assume  $c_{ii} = 0$  ( $i = 1, 2, \dots, N$ ), regarding self-couplings as intrinsic dynamics, and we do not infer the self-coupling  $c_{ii}$ .

Here, we summarize the algorithm of the naive method. Let us assume that an oscillatory signal is observed at  $K$  time steps,  $y_{i,k} = y_i(kh)$  ( $k = 0, 1, \dots, K-1$ ), where  $h$  is the sampling interval. The naive method consists of the following two steps (Fig. 1):

- (i): Reconstruct the phase  $\{\phi_{i,k}\}$  ( $k = 0, 1, \dots, K-1$ ) from the observed data  $\{y_{i,k}\}$  ( $k = 0, 1, \dots, K-1$ ) by using Hilbert transform [1, 45] for oscillator  $i$  ( $i = 1, \dots, N$ ). See Appendix B for details of implementation.
- (ii): Infer the parameters in Eq. (12) including the coupling strength  $\{c_{ij}\}$  ( $i, j = 1, 2, \dots, N$ ) from the reconstructed phase  $\{\phi_{i,k}\}$  by maximizing the log-likelihood function. The expression for the log-likelihood function and the maximization procedure is summarized in Appendix B.

Although this naive method is a straightforward way to infer the oscillator network, it is important to recognize the following two potential sources of error.

**A:** Due to the averaging approximation, there is a discrepancy of  $O(\epsilon)$  between the non-averaged model (4) and the averaged model (5) used for inference.

**B:** A rapid phase change may not be accurately reconstructed from observed signals via Hilbert transform [46].

In the following subsections A and B, we examine the effect of the averaging approximation and the effect of the phase reconstruction on the performance of the naive method, respectively.

### A. Effect of averaging approximation

The averaging approximation simplifies the model in two aspects: 1) the natural frequency is constant, and 2) the interaction term is a function of the phase difference. Here we examine the effect of the averaging approximation by

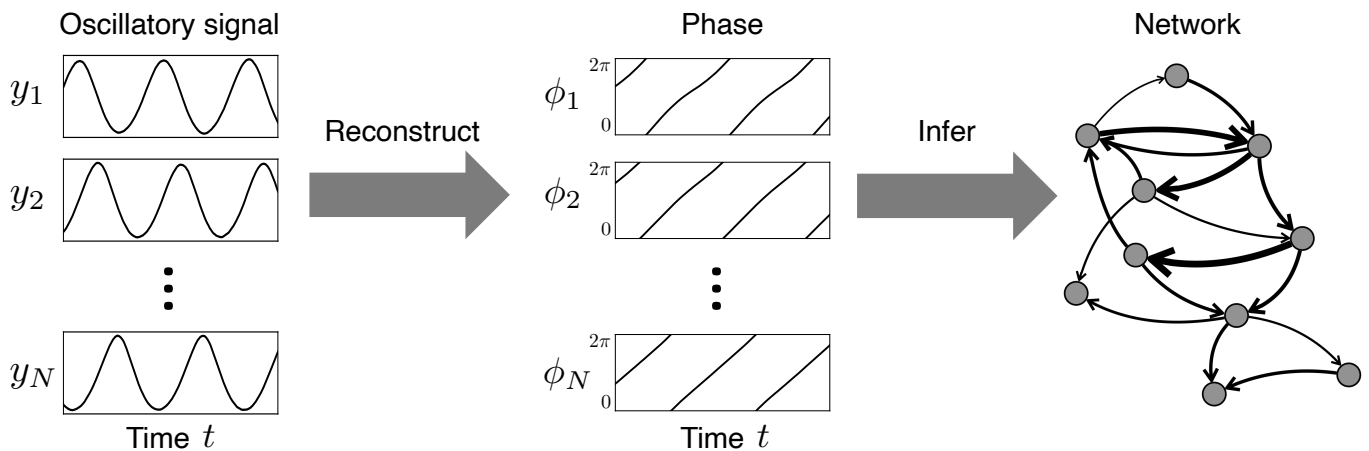


FIG. 1. Procedure for network inference of an oscillator system. (i) Reconstructing the phase signals  $\phi_i(t)$  from the observed signals  $y_i(t)$ . (ii) Inferring the interaction network from the phase signals. The direction and the width of the arrow represent the direction and the weight of the network, respectively.

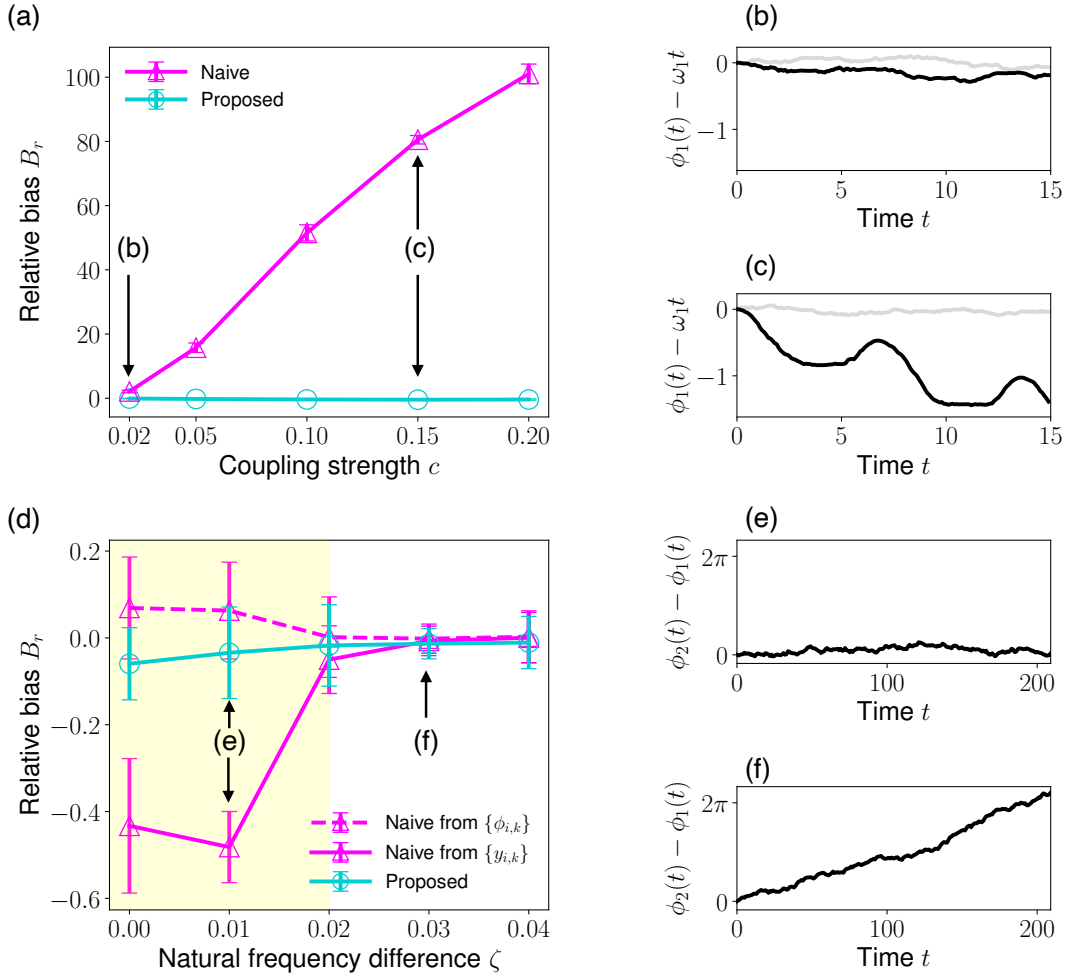


FIG. 2. Difficulties in the inference of the oscillator network.

(a-c): Effect of averaging approximation. (a): Mean and standard deviation of the relative bias  $B_r$  of the naive method (magenta) and the proposed method (cyan). (b) and (c): Phase time series at coupling strength  $c = 0.02$  (b) and  $0.15$  (c). The phase of the true model (13, 14) and the averaged model (12) are shown in black and grey, respectively. Note that we subtracted the natural frequency component  $\omega_i t$  from the phase  $\phi_i(t)$ . Parameters of stochastic Winfree oscillators (13, 14) are  $\omega_1 = \omega_2 = 1.0$  and  $\sigma_1 = \sigma_2 = 0.05$ .

(d-f): Effect of phase reconstruction. (d): Mean and standard deviation of the relative bias of the naive method (magenta) and the proposed method (cyan). The yellow indicates the region where the oscillators are synchronized in the absence of noise. (e) and (f): Phase time series at the natural frequency difference  $\omega_2 - \omega_1 = 0.0$  and  $0.04$ . Parameters of stochastic Kuramoto model are  $\omega_1 = 1.0$ ,  $c = 0.01$ , and  $\sigma_1 = \sigma_2 = 0.01$ .

applying the naive method to synthetic data generated by a non-averaged model. As a minimal model, we consider a system of two phase oscillators as the true model:

$$\frac{d\phi_1}{dt} = \omega_1 - 2c \sin \phi_1 (1 + \cos \phi_2) + \sigma_1 \sin \phi_1 \xi_1(t), \quad (13)$$

$$\frac{d\phi_2}{dt} = \omega_2 - 2c \sin \phi_2 (1 + \cos \phi_1) + \sigma_2 \sin \phi_2 \xi_2(t), \quad (14)$$

where,  $\omega_{1,2}$  is the natural frequency,  $c$  is the coupling strength, and  $\sigma_{1,2}$  represents noise strength. This model is a stochastic Winfree model [2, 47], and it is a non-averaged phase model (4) with  $\epsilon \nu_i(\phi_i) = \omega_i - \omega$ ,  $\epsilon q_{ij}(\phi_i, \phi_j) = -2c \sin \phi_i (1 + \cos \phi_j)$ , and  $Z(\phi_i) = \sin \phi_i$ . By applying the averaging approximation, we can obtain the model (12) used for the inference from the true model model (13, 14) (see Appendix C for the derivation). Consequently, it can be expected that the naive method will achieve accurate inference when coupling and noise are sufficiently weak.

We examine the dependency of the inference performance on the coupling strength  $c$ . We first generate the phase time series  $\{\phi_{i,k}\}$  ( $i = 1, 2$ ) by simulating the true model (13, 14) using Euler-Maruyama method with a time step of

0.01. Then, we infer the coupling strengths ( $c_{12}$  and  $c_{21}$ ) from the phase time series using the naive method (step ii). Note that it is assumed that the true phase signal is observable to eliminate the effect of the phase reconstruction. We evaluate the inference performance by using the relative bias defined as  $B_r = (\hat{c}_{ij} - c_{ij})/c_{ij}$ , where  $c_{ij}$  and  $\hat{c}_{ij}$  are the true coupling strength and its inferred value, respectively. As shown in Fig.2a (magenta), the inference performance deteriorates rapidly as the coupling strength increases. The naive method tends to overestimate the coupling strength. For the coupling strength of  $c = 0.15$ , the naive method infers the coupling strength to be 81 times larger than the true value. It is noteworthy that the inference is not accurate even for a weak coupling of  $c = 0.05$ , where the inferred value is, on average, more than 10 times larger than the true value.

Furthermore, we compare the phase of the true model (13, 14) with that of the averaged model (12) used for the inference. When the coupling strength is very small ( $c = 0.01$ ), the true model (Fig. 2b, black) exhibits similar behavior to the averaged model (Fig. 2b, grey). In contrast, when the coupling strength is large ( $c = 0.15$ ), the behavior of these models is markedly different. While the phase of the true model varies periodically (Fig. 2c, black), the phase of the averaged model exhibits no such periodic variation (Fig. 2c, grey). This discrepancy between the true model and the averaged model used in the naive method could yield a large error in the inference.

## B. Effect of phase reconstruction

In most cases, the phase itself is not directly observable, and thus it is necessary to reconstruct the phase from the observed data. Commonly, the phase reconstruction is not perfect. For example, the Hilbert transform method cannot accurately reconstruct rapid fluctuations in phase, even if the observed signal is sinusoidal-like waveform [46]. To examine the effect of the phase reconstruction error on the coupling inference, we assume that the observed data is the sinusoidal-like signal:  $y_i(t) = \cos \phi_i(t)$ . Note that we do not consider the cases where the waveform is more complex, such as when it contains higher harmonics. Several methods are proposed to reconstruct the phase from complex signals [30, 48], whereas these methods might have a similar limitation since they are also based on the Hilbert transform.

Here we consider the averaged model (5) as the true model to focus on the effect of phase reconstruction and exclude the effect of averaging approximation (Sec. III A). As a minimal model, we consider a system of two phase oscillators as the true model:

$$\frac{d\phi_1}{dt} = \omega_1 + c \sin(\phi_2 - \phi_1) + \sigma_1 \xi_1(t), \quad (15)$$

$$\frac{d\phi_2}{dt} = \omega_2 + c \sin(\phi_1 - \phi_2) + \sigma_2 \xi_2(t), \quad (16)$$

where  $\omega_{1,2}$  is the natural frequency,  $c$  is the coupling strength, and  $\sigma_{1,2}$  represents the noise strength. This is a stochastic Kuramoto model [1] that is an averaged model (5) with the sinusoidal coupling function (11) for  $N = 2$ . Consider the case of no noise ( $\sigma_1 = \sigma_2 = 0$ ) and the positive coupling ( $c > 0$ ). The synchronization state of this model is determined by the natural frequency difference  $\zeta := \omega_2 - \omega_1$ . Specifically, the two oscillators are synchronized or phase-locked if the difference in natural frequencies is less than a critical value:  $|\zeta| < 2c$ , otherwise they are asynchronous. Hence we can easily control the synchronization state by changing the natural frequency difference.

We examine the dependency of the inference performance on the natural frequency difference. We first generate the synthetic data to evaluate the inference performance. The phase time series  $\{\phi_{i,k}\}$  ( $i = 1, 2; k = 0, 1, \dots, K-1$ ) are generated by applying Euler-Maruyama method to Eqs. (15, 16) with a time step of 0.01. Then, we generate the synthetic signal based on the phase:  $y_{i,k} = \cos \phi_{i,k}$ . We quantify the inference performance by the relative bias  $B_r$  for different values of the natural frequency difference. Fig. 2d compares the performance of the naive method from the observed signal  $\{y_{i,k}\}$  (solid magenta line) with that from the true phase  $\{\phi_{i,k}\}$  (dashed magenta line). When we infer the coupling strength from the signal, the inference performance degrades for small natural frequency differences  $\zeta$ . The naive method performs well for  $\zeta = 0.02, 0.03$  and  $0.04$ , whereas this method considerably underestimates the coupling strength for  $\zeta = 0.00$  and  $0.01$ . The border is around  $\zeta = 0.02$ , which is actually the critical value  $2c$  between synchrony and desynchrony for the noiseless oscillators. Furthermore, it was confirmed that the oscillators exhibited synchronous/desynchronous activity when the natural frequency differences were smaller/larger than the critical value (Figs. 2e and f). In contrast, when we infer the coupling strength from the true phase, the bias is small regardless of the natural frequency difference  $\zeta$ . This result suggests that the phase reconstruction has a significant negative impact on the coupling inference when the oscillators synchronize.

Finally, we explain the reason why the phase reconstruction of the naive method negatively affect the coupling inference from the synchronized oscillators. It is essential to reconstruct the short-time phase change  $\delta\phi_{i,k}$  (12) for inferring the coupling. When the oscillators synchronize, the phase change fluctuates rapidly since the coupling term  $\sin(\phi_{2,k} - \phi_{1,k})$  is nearly constant (Fig. 2e) and the noise term  $\xi_{i,k}$  dominates the phase change. Because of the

properties of the Hilbert transform [46], the rapid fluctuation in the phase change is smoothed out, which degrades the coupling inference. In contrast, when the oscillators desynchronize, the phase change  $\delta\phi_{i,k}$  varies slowly since the coupling term  $\sin(\phi_{2,k} - \phi_{1,k})$  changes in the range of  $[-1.0, 1.0]$  (Fig. 2f). Since the slow fluctuation is less susceptible to the smoothing effect of the Hilbert transform, the precise inference is achieved when the oscillators desynchronize.

### C. Summary

We describe the naive method for inferring the network of oscillators from observed signals. It is demonstrated that the performance of the naive method is impaired due to the errors accompanied by the averaging approximation and the phase reconstruction, and it is valid only when the couplings are very weak and when the oscillators desynchronize. With respect to the phase reconstruction (Sec. III B), this issue can be resolved by employing a more sophisticated technique other than the naive Hilbert transform, such as the iterative Hilbert transform [48] and the extended Hilbert transform [46]. However, the first issue regarding the averaging approximation (Sec. III A) is fundamental: we infer the coupling strength of  $O(\epsilon)$  using a model that can deviate  $O(\epsilon)$  from the true model (i.e., a system of weakly coupled limit-cycle oscillators). It is challenging to avoid this issue as far as we employ the averaged equation (5) used for the inference.

## IV. PROPOSED METHOD

We propose a method for inferring the interaction network based on the circle map, which describes the evolution of the phase over a period of an oscillator [1]. Consider the change in phase  $\phi_i(t)$  of oscillator  $i$  from time  $t$  to  $t + T$ , where  $T = 2\pi/\omega$  represents the typical period of an oscillator. We can derive the circle map from the phase equation (4) under the assumption of weak coupling  $O(\epsilon)$  (see Appendix D for details):

$$\phi_i(t + T) - \phi_i(t) = T\omega_i + T \sum_{j=1}^N c_{ij} \gamma_{ij} (\phi_j(t) - \phi_i(t)) + \sqrt{T} \sigma_i \xi_{i,t} + O(\epsilon^2), \quad (17)$$

where  $c_{ij}$  is the coupling strength from oscillator  $j$  to  $i$ ,  $\gamma_{ij}(\phi_j(t) - \phi_i(t))$  is the averaged coupling function, and  $\xi_{i,t}$  are the independent gaussian random variables with mean 0 and variance 1. The error yielded by the derivation is  $O(\epsilon^2)$ , which shows that the circle map (17) is better approximation than the averaged equation (5).

Similar to the naive method, we obtain the model that is used for the inference of the proposed method by assuming the sinusoidal function for the coupling function (11) and discretizing it:

$$\Delta\Phi_{i,m} = T\omega_i + T \sum_{j=1}^N c_{ij} \sin(\Phi_{j,m} - \Phi_{i,m} + \alpha) + \sqrt{T} \sigma_i \xi_{i,m}, \quad (18)$$

where  $m$  is a discrete time step ( $m = 0, 1, \dots, M - 1$ ),  $\Phi_{i,m} = \phi_i(mT)$ ,  $\Delta\Phi_{i,m} = \Phi_{i,m+1} - \Phi_{i,m}$  is the phase change over the typical period  $T$ ,  $\sigma_i^2$  is the averaged noise variance (9), and  $\xi_{i,m}$  an independent Gaussian random variable with mean 0 and variance 1.

Subsequently, we infer the parameters  $\alpha, \{\omega_i\}, \{c_{ij}\}$  ( $i, j = 1, 2, \dots, N$ ) by maximizing the log-likelihood function. The log-likelihood function that corresponds to Eq. (18) is given as

$$l(\alpha, \boldsymbol{\theta}_1, \boldsymbol{\theta}_2, \dots, \boldsymbol{\theta}_N) = \sum_{i=1}^N l_i(\alpha, \boldsymbol{\theta}_i), \quad (19)$$

$$l_i(\alpha, \boldsymbol{\theta}_i) = -\frac{M}{2} \log(2\pi\sigma_i^2 T) - \frac{1}{2\sigma_i^2 T} \sum_{m=0}^{M-1} \left( \Delta\Phi_{i,m} - T \left\{ \omega_i + \sum_{j=1}^N c_{ij} \sin(\Phi_{j,m} - \Phi_{i,m} + \alpha) \right\} \right)^2, \quad (20)$$

where,  $l_i(\alpha, \boldsymbol{\theta}_i)$  and  $\boldsymbol{\theta}_i := (\omega_i, c_{i1}, c_{i2}, \dots, c_{iN}, \sigma_i)$  are the log-likelihood and set of parameters associated with oscillator  $i$ . Due to the parameter  $\alpha$  in Eq.(20), the log-likelihood function is not quadratic in terms of the parameters, rendering its maximization nontrivial. However, for a fixed value of  $\alpha$ , we can maximize the function  $l_i(\alpha, \boldsymbol{\theta}_i)$  by solving a set of linear equations to find the optimal parameter set:

$$\hat{\boldsymbol{\theta}}_i(\alpha) = \arg \max_{\boldsymbol{\theta}_i} l_i(\alpha, \boldsymbol{\theta}_i). \quad (21)$$

Thus, the maximization of the log-likelihood function (19) can be reduced to an optimization problem of the scalar function of one variable:

$$\tilde{l}(\alpha) = \sum_{i=1}^N l_i(\alpha, \hat{\boldsymbol{\theta}}_i(\alpha)). \quad (22)$$

This optimization problem can be efficiently solved by using the Brent method [49] in a range of  $-\pi/2 < \alpha \leq \pi/2$ .

Here, we describe the procedure of the propose method. Assume that an oscillatory signal is observed at  $K$  time steps,  $y_{i,k} = y_i(kh)$ , where  $h$  is the sampling interval same as the naive method. The proposed method consists of three steps.

- (i) As with the naive method, reconstruct the phase  $\{\phi_{i,k}\}$  of each oscillator from the observed data  $\{y_{i,k}\}$  ( $i = 1, 2, \dots, N; k = 0, 1, \dots, K-1$ ) by using the Hilbert transform.
- (ii) Estimate the typical period  $T$ . We first calculate the average period  $\langle \tau \rangle = \frac{1}{N} \sum_{i=1}^N \tau_i$ , where  $\tau_i = \left( \frac{\phi_{i,K} - \phi_{i,0}}{2\pi h K} \right)^{-1}$  is the period of oscillator  $i$ . We then estimate the typical period  $T$  by  $\hat{T} = Lh$ , where  $L$  is an integer nearest to  $\frac{\langle \tau \rangle}{h}$ .
- (iii) Determine the parameters  $(\alpha, \boldsymbol{\theta}_1, \boldsymbol{\theta}_2, \dots, \boldsymbol{\theta}_N)$  by maximizing the log-likelihood (19). First, we fix a parameter  $\alpha$  and optimize the other parameters by solving a set of linear equations. Then, we optimize  $\alpha$  by maximizing Eq. (22) using the Brent method.

Note that, if the number of the oscillators are large enough:  $\log K \ll N^2$ , the proposed method is computationally faster than the naive method. The computational complexity of the naive and the proportional method are approximately  $O(KN^2)$  and  $O(MN^2)$ , respectively.

The proposed method is expected to be more robust against the two sources of error of the naive method mentioned in Sec. III. The averaging approximation can negatively affect the inference performance because there is a difference of  $O(\epsilon)$  between the non-averaged phase model (4) reduced from the weakly coupled limit-cycle oscillators and the averaged phase model (5) used in the naive method. In contrast, there is a difference of  $O(\epsilon^2)$  between the non-averaged phase model (4) and the circle map (17) used in the proposed method. Therefore, the proposed method is expected to reduce the error due to the averaging approximation. Moreover, the proposed method is less susceptible to the low-pass filter effect of the Hilbert transform because the proposed method is based on the phase change over a typical period  $T$ , which is much larger than the original sampling interval  $h$ .

Now, we demonstrate that the proposed method can solve the two problems (Sec. III A and B). We first apply the proposed method to the phase time series generated by the stochastic Winfree model (13, 14). Fig. 2a (cyan) shows that the proposed method performs excellently even when the coupling is not very weak. For instance, for the coupling strength of  $c = 0.15$ , the phases of the averaged equation considerably deviates from that of the non-averaged equation (Fig. 2c), and the naive method is unable to infer the coupling strength accurately. The mean relative bias and the squared error of the naive method are 81 and 146, respectively. Nevertheless, the proposed method accurately infers the coupling strength. The mean relative bias and the squared error the proposed method are  $-0.45$  and  $0.0050$ , respectively. Next, we apply the proposed method to the synthetic data  $y_{i,k} = \cos \phi_{i,k}$ , where the phase  $\phi_{i,k}$  is generated by the stochastic Kuramoto model (15, 16). Fig. 2d (cyan) shows that the proposed method performs well even when the oscillators are in a synchronized state. For instance, for the phase difference of  $\zeta = 0.01$ , the two oscillators are strongly synchronized (Fig. 2e), and the naive method is unable to infer the coupling strength accurately. The mean relative bias and the squared error of the naive method are  $-0.48$  and  $2.4 \times 10^{-5}$ , respectively. Again, the proposed method accurately infers the coupling strength. The mean relative bias and the squared error the proposed method are  $-0.034$  and  $1.2 \times 10^{-6}$ , respectively.



## V. APPLICATIONS

In Sec. IV, we have demonstrated that the proposed method is robust against the two sources of error of the naive method (i.e., the averaging approximation and the phase reconstruction) using the data generated by the phase models. Here, we test the validity of the proposed methods using the data obtained from limit-cycle oscillators, which are more realistic models compared to the phase models. In particular, we consider two models: the Brusselator model for chemical oscillators and the model of circadian oscillators in the suprachiasmatic nucleus (SCN).

### A. Brusselator oscillators

We consider a network of 10 Brusselator oscillators [50], described by

$$\frac{dx_i}{dt} = A_i + x_i^2 y_i - (B_i - 1)x_i + \sum_{j=1}^N K_{ij}(x_j - x_i) + \rho \xi_i^{(x)}(t), \quad (23)$$

$$\frac{dy_i}{dt} = B_i x_i - x_i^2 y_i + d \sum_{j=1}^N K_{ij}(y_j - y_i) + \rho \xi_i^{(y)}(t), \quad (24)$$

where  $x_i(t)$  and  $y_i(t)$  represent the state of oscillator  $i$ ,  $K_{ij}$  represents the coupling strength from oscillator  $j$  to oscillator  $i$ ,  $\xi_i^{x,y}(t)$  are the independent Gaussian white noise with mean 0 and variance 1. In order to model the heterogeneity between oscillators, the parameter  $A_i$  was drawn from the uniform distribution [0.9999, 1.0001] and  $B_i$  was set to  $B_i = (1 + \mu)(1 + A_i^2)$ , where  $\mu$  is the Hopf bifurcation parameter. In this case, each unit behaves as a limit-cycle oscillator when  $\mu > 0$ . The other parameters are set as follows:  $d = 1.25$  and  $\rho = 0.002$ . Here, we consider a network composed of two groups of oscillators: a densely connected population (Fig. 3b, d: left) and a sparsely connected population (Fig. 3b, d: right). The coupling strength,  $K_{ij}$ , is set to  $K_{ij} = 0.001$  if there is a directed edge from oscillator  $j$  to  $i$ , and  $K_{ij} = 0.0$  otherwise. The simulated data were generated using the Euler-Maruyama method with a time step of 0.01.

From the observed signal  $x_i(t)$  ( $i = 1, 2, \dots, 10$ ), we infer the coupling network  $\{c_{ij}\}$  ( $i, j = 1, 2, \dots, 10$ ) of the averaged phase model (5) that is expected to be approximately proportional to the coupling in the Brusselator oscillators (23, 24). The sampling interval of the observed signal is set to  $h = 0.01$ , and the observation duration is set to  $T = 3.0 \times 10^5$  (approximately  $5 \times 10^4$  periods). In the naive method, the sampling interval is set to  $h = 0.1$  because otherwise the computational cost will be enormous. It was confirmed that the results are quantitatively preserved from the case of  $h = 0.01$  using several shorter data sets. First, we consider the case of  $\mu = 0.001$ , which is rather close to the Hopf bifurcation point. The waveform of the observed signal is close to a sinusoidal wave, but the amplitude of the oscillators varies due to the heterogeneity (Fig.3a). Fig.3b compares the true network (top) with the inferred results from the observed signals using the naive method (middle) and the proposed method (bottom). The naive method is unable to infer the true network structure and the relative weights. Notably, the naive method infers negative coupling strengths in the left populations, whereas the true couplings are positive. Moreover, the naive method infers that the left network is much more strongly connected than the right network, despite the identical coupling strengths of the left and right networks. In contrast, the proposed method is able to infer the network accurately. The correlation coefficient between the true coupling network and its estimate was  $-0.77$  for the naive method and  $0.96$  for the proposed method. This result indicates that the proposed method achieves a better inference result than the naive method.

Second, we test whether the proposed method is applicable to the case when the waveform of the observed signal is distorted from a sinusoidal waveform (Fig.3c) and the coupling function  $\gamma(\theta_j - \theta_i)$  deviates from the sinusoidal function. For this purpose, we examine the case of  $\mu = 0.04$ , which is not very close to the Hopf bifurcation point. Similar to Fig.3b, Fig.3d compares the true network (top) with the inferred results using the naive method (middle) and the proposed method (bottom). While the naive method cannot infer the connections in the sparse network (right group), the proposed method infers the network structure accurately. The correlation coefficient between the true coupling matrix and its estimate was  $0.75$  for the naive method and  $0.98$  for the proposed method. Again, this result demonstrates that the proposed method achieves a superior inference result than the naive method in this case as well.

We note that the left group is well synchronized in both cases  $\mu = 0.001$  and  $\mu = 0.04$ , and the proposed method performs well even for synchronized oscillators. To show this, we quantify the degree of synchronization by a group-

level Kuramoto order parameter

$$R_u = \left\langle \left| \frac{1}{N_u} \sum_{j \in \mathcal{A}_u} e^{i\phi_j(t)} \right| \right\rangle \quad (25)$$

where  $u \in \{1, 2\}$  indicates the left ( $u = 1$ ) or the right ( $u = 2$ ) group in Fig.3b and d. Each group has  $N_u = 5$  oscillators and the set of the oscillators' indices is denoted by  $\mathcal{A}_u$ . The group-level order parameter takes its maximum value  $R_u = 1$  when the oscillators in the group completely synchronize in phase, while it takes its minimum value  $R_u = 0$  when the oscillators' phases are uniformly distributed. We obtain  $(R_1, R_2) = (0.97, 0.55)$  for  $\mu = 0.001$ , and  $(R_1, R_2) = (1.00, 0.62)$  for  $\mu = 0.04$  showing the high synchrony in the left group. This result demonstrates that the proposed method is able to extract the network structure from oscillatory signals even when the oscillators are in a highly synchronous state.

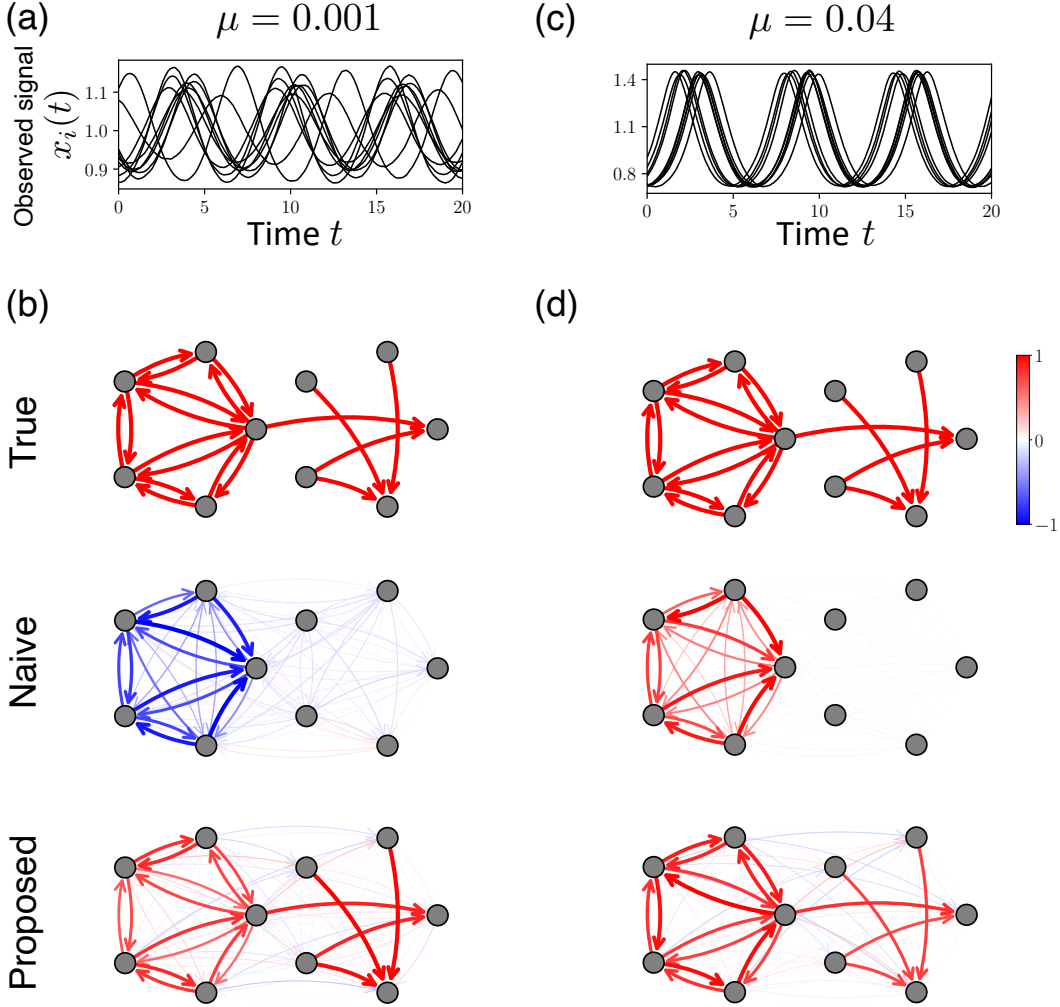


FIG. 3. Network inference from oscillatory signals: Application to simulated data from Brusselator oscillators. (a): Observed signals  $x_i(t)$  generated by Brusselator oscillators whose bifurcation parameter is close to Hopf bifurcation point:  $\mu = 0.001$ . (b): True network between Brusselator oscillators (top) and networks inferred from the observed signals (a) by the naive method (middle) and the proposed method (bottom). (c): Same as (a), but the data is simulated with the bifurcation parameter that is not very close to the Hopf bifurcation point:  $\mu = 0.04$ . (d): Same as (b), but the network was inferred from the observed signals (c). In (b) and (d), the relative weights of the couplings are represented by the color and width of the arrows.

## B. Clock cells oscillators

A second example is the network of clock cells. The mammalian circadian rhythm is driven by genetic oscillations in the clock cells, the neurons composing the SCN. However, it is still unclear how the clock cells interact with each other to produce a stable rhythm [51]. In particular, the interaction between two anatomically distinct subregions of the SCN (i.e., the core and shell regions) has attracted attention because it is thought to play an important role in generating robust rhythmic signals [52]. Here, we consider a toy model of the SCN. As illustrated in Fig. 4, we consider a clock-cell network composed of two densely connected subregions (1 and 2 in Fig. 4) and assume two inter-group connections. Using synthetic data generated by this model, we investigate the performance of our methods in inferring the intra- and inter-networks of two subregions. We employ the model and parameters proposed in [53] as a clock cell and consider its network, as proposed in [54], given by

$$\frac{dx_i}{dt} = \tau_i \left( v_1 \frac{K_1^n}{K_1^n + z_i^n} - v_2 \frac{x_i}{K_2 + x_i} + v_c \frac{F_i}{K_c + F_i} \right) + \rho \xi_i^x(t), \quad (26)$$

$$\frac{dy_i}{dt} = \tau_i \left( k_3 x_i - v_4 \frac{y_i}{K_4 + y_i} \right) + \rho \xi_i^y(t), \quad (27)$$

$$\frac{dz_i}{dt} = \tau_i \left( k_5 y_i - v_6 \frac{z_i}{K_6 + z_i} \right) + \rho \xi_i^z(t), \quad (28)$$

$$\frac{dr_i}{dt} = \tau_i \left( k_7 x_i - v_8 \frac{r_i}{K_8 + r_i} \right) + \rho \xi_i^r(t), \quad (29)$$

where  $x_i$ ,  $y_i$ ,  $z_i$ , and  $r_i$  (nM) represent the concentration of mRNA, a clock protein, a transcriptional repressor, and a neuropeptide of clock cell  $i$ , respectively, and  $\xi_i^{x,y,z,r}(t)$  represent the independent gaussian white noise. The Hill coefficient is set to  $n = 5$  and the scaling factor  $\tau_i$  is drawn from the uniform distribution  $[0.9999, 1.0001]$  to incorporate the heterogeneity in the clock cells. The simulated data were generated using the Euler-Maruyama method with a time step of 0.04. Other parameters are summarized in Table I.

$F_i$  represents the interaction between the clock cell models and is defined as following [54]:

$$F_i = \sum_{j=1}^N A_{ij} r_j, \quad (30)$$

where  $A_{ij}$  represents the coupling strength from clock cell model  $j$  to  $i$ . The coupling strength is set to  $A_{ij} = 0.01$  when there is a coupling from the clock cell model  $j$  to  $i$ ; otherwise,  $A_{ij} = 0.0$ . The self-coupling was set to  $A_{ii} = 0.9$  ( $i = 1, 2, \dots, 10$ ) to allow the clock cell model to oscillate autonomously even in the absence of coupling.

We inferred the coupling network  $\{c_{ij}\}$  ( $i, j = 1, 2, \dots, 10$ ) from the observed signal  $y_i(t)$  ( $i = 1, 2, \dots, 10$ ) obtained from the clock cell model (Eqs. 26–29). The sampling interval of the observation data was  $h = 0.04$ , and the observation duration was  $T = 1.2 \times 10^6$  (approximately  $5 \times 10^4$  periods). In the naive method, the sampling interval was  $h = 0.4$  because otherwise the computational cost will be enormous. It was confirmed that the results are quantitatively preserved from the case of  $h = 0.04$  using several shorter data sets.

In this subsection, we consider three cases of interaction between groups of clock cells as follows: a) no interaction (Fig.4a), b) one-way or unidirectional interaction (Fig.4b), and c) two-way or bidirectional interaction (Fig.4c). We calculated the group-level Kuramoto order parameter  $R_u$  (25) from the clock cells in the left ( $u = 1$ ) and right ( $u = 2$ ) groups. The oscillators in each group are highly synchronized: the order parameter obtained from the left and right groups was 0.99 and 0.98 in the case of no interaction (Fig.4a), 0.99 and 0.99 in the case of one-way interaction (Fig.4b), and 0.99 and 0.99 in the case of two-way interaction (Fig.4c). Next, we obtain the phase  $\theta_i(t)$  from the time series  $x_i(t)$  ( $i = 1, 2, \dots, 10$ ) using the Hilbert transform and infer the coupling network. To evaluate the performance

TABLE I. Parameters of the clock cell model.

Parameters	Values		
$v_1, v_2, v_c$ [nM/h]	6.8355,	8.4297,	6.7924
$v_4, v_6, v_8$ [nM/h]	1.0841,	4.6645,	3.5216
$K_1, K_2, K_c$ [nM]	2.7266,	0.2910,	4.8283
$K_4, K_6, K_8$ [nM]	8.1343,	9.9849,	7.4519
$k_3, k_5, k_7$ [/h]	0.1177,	0.3352,	0.2282

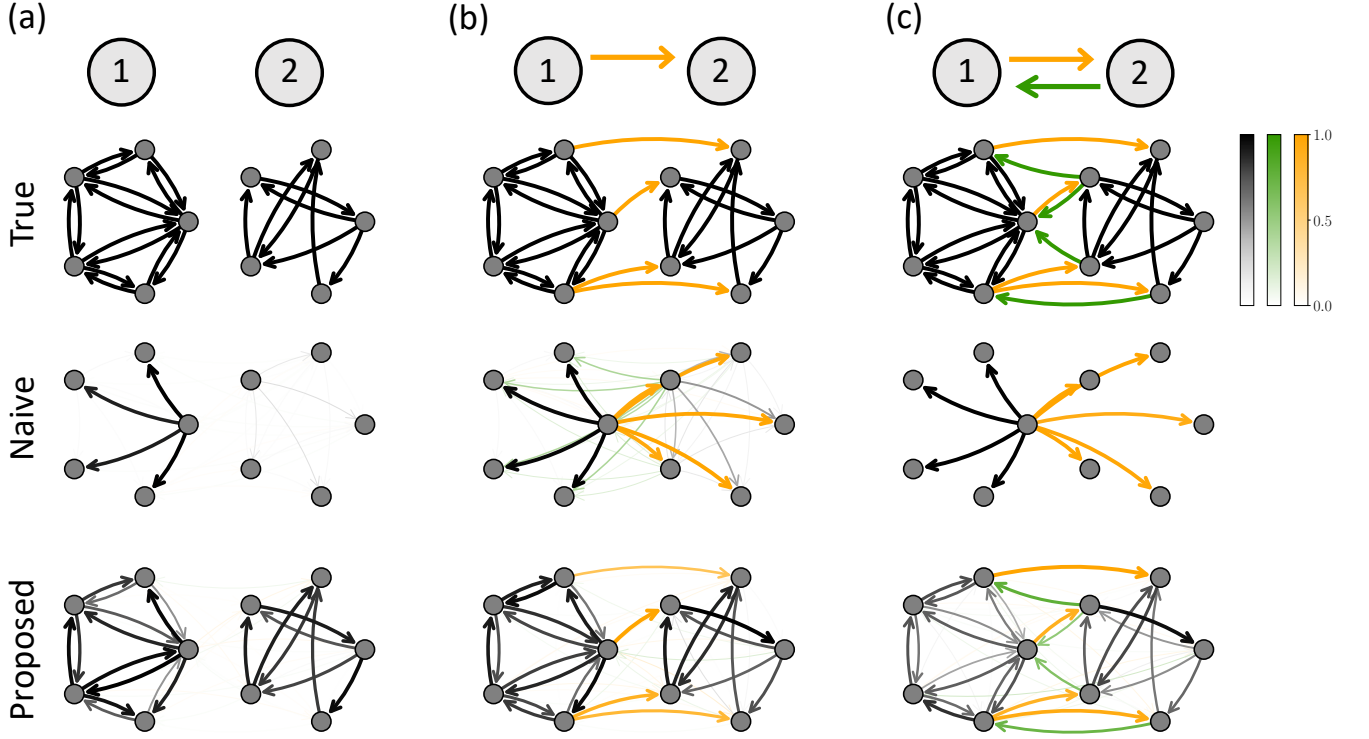


FIG. 4. Network inference from oscillatory signals: Application to synthetic data by coupled SCN model neurons. Inference results for three network structures are shown, (a): no connection between two groups, (b): unidirectional connections between two groups, i.e., the interactions are from the neurons in the right group to those in the left group, and (c): bidirectional connections between two groups. True interaction networks are shown in the top panels. Inferred networks from observations  $y_i(t)$  (Eq. 27) by the naive method and the proposed method are shown in the middle and bottom panels, respectively. The relative weights of the couplings are represented by the color and width of the arrows.

of the inference, we calculate the correlation coefficient between the estimated network and the true network in the clock cell model. The correlation coefficient of the naive method and the proposed method was 0.23 and 0.98 in the case of no interaction (Fig.4a), 0.053 and 0.97 in the case of one-way interaction (Fig.4b), and 0.14 and 0.95 in the case of two-way interaction (Fig.4c). This result suggests that the proposed method can infer the oscillator network much more accurately than the naive method.

The inference results (Fig.4) suggest that the proposed method is able to extract the inter- and intra-group interactions from the data, whereas the naive method fails to capture these interactions. To quantify this, we define the connectivity between the groups of oscillators as follows:

$$C_{uv} = \frac{1}{|C|} \sum_{i \in \mathcal{A}_u} \sum_{j \in \mathcal{A}_v} c_{ij}, \quad (31)$$

where  $\mathcal{A}_u$  is the set of oscillator indices in group  $u \in \{1, 2\}$ , and  $|C| := \sum_{i \in \mathcal{A}_u} \sum_{j \in \mathcal{A}_v} |c_{ij}|$  is the sum of the absolute values of inferred coupling strengths. Fig.5 shows the group level connectivity  $C_{uv}$  of the true and inferred networks. The inferred network by the naive method has much smaller  $C_{11}$  and  $C_{22}$  than the true network. This result indicates that the naive method cannot extract a densely connected group of clock cells. In contrast, the inferred network by the proposed method has similar  $C_{11}$  and  $C_{22}$  to the true network. Furthermore, the inferred results of the proposed method can reproduce the group-level connectivity ( $C_{12}$  and  $C_{21}$ ) of the true network. These results indicate that the proposed method can extract not only a densely connected group of clock cells, but also the direction of interaction (e.g., one-way or two-way) between the groups.

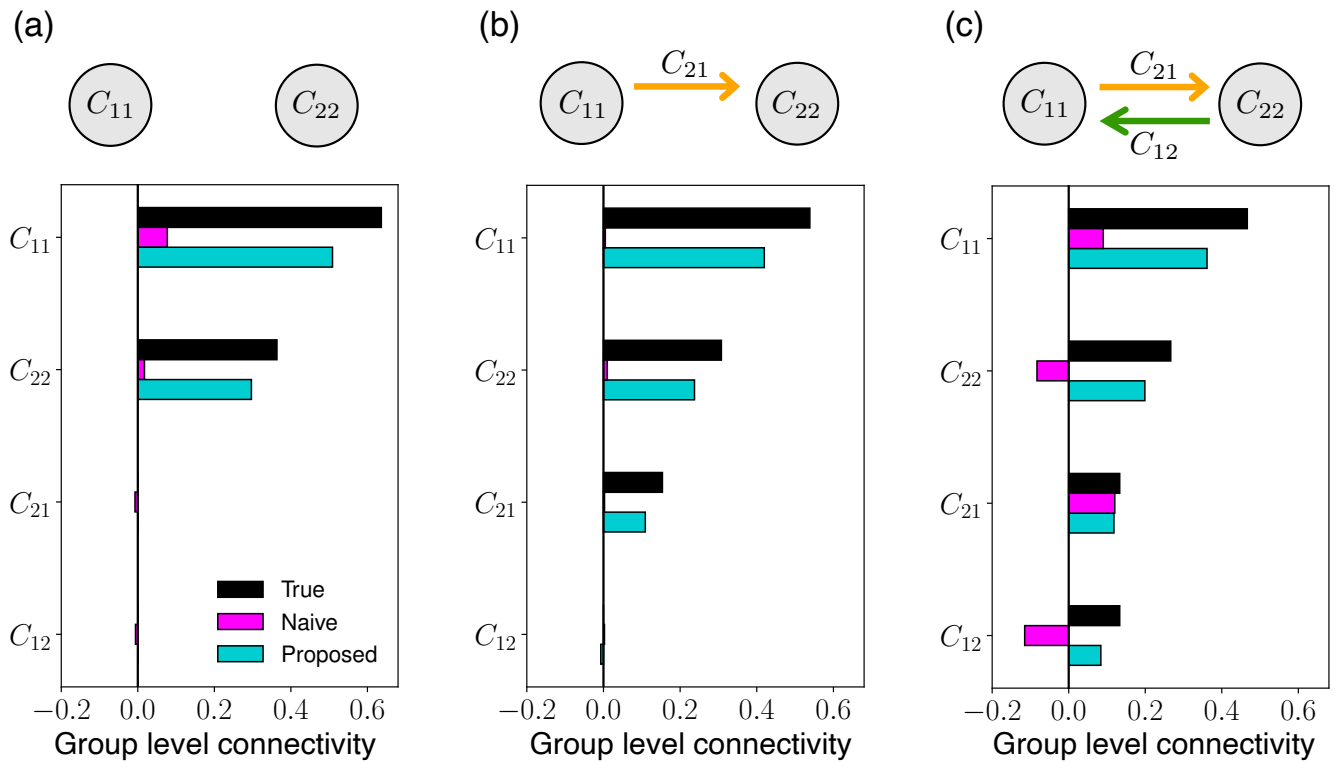


FIG. 5. Group-level connectivity  $C_{uv}$  between the clock cell groups.

We compared the group-level connectivity from cell group  $v$  to cell group  $u$  of the true network with that of the inferred network by the naive and proposed method ( $u, v = 1, 2$ ). Same as Fig. 4, we show three networks: (a) no interaction between cell groups, (b) one-way interaction between cell groups, (c) two-way interaction between cell groups. Parameters are same as Fig. 4.

## VI. DISCUSSION

We have proposed a method for inferring the network of coupled oscillators from the observed signal. In our approach, the phase is first reconstructed from the observed signal, and then the interaction network (i.e., coupling network) is inferred from the phase (Fig. 1). This method infers the coupling network  $\{c_{ij}\}$  ( $i, j = 1, 2, \dots, N$ ) of the averaged phase equation (5) by fitting the parameters of the circle map. First, we have demonstrated that this method can accurately infer the network even when the oscillator dynamics cannot be described by the averaged phase model or when the oscillators are synchronized (Fig. 2). We have subsequently validated the proposed method using simulated data from limit-cycle oscillators, i.e., the Brusselator oscillator and the clock cell model (Figs. 3 and 4). Furthermore, the result of the clock cell model (Fig. 5) suggests that the proposed method can extract the group structure of the coupling network and the interaction between groups.

Methods for inferring the coupling of oscillators can be classified into two approaches: (i) fitting the coupling function  $q(\phi_i, \phi_j)$  [33, 55] and (ii) fitting the averaged coupling function  $\gamma(\phi_i - \phi_j)$  [29, 34, 56]. The proposed method belongs to the latter approach. The latter approach has the advantage that it can infer the coupling network and requires less data. However, the existing methods in this approach have limited accuracy, except when applied to a narrow class of systems, such as the Kuramoto model. This is because this approach is based on the averaged phase equation (5), which can deviate  $O(\epsilon)$  from the original dynamical system (Sec. II). In contrast, the proposed method is based on a circle map that deviates from the original system by only  $O(\epsilon^2)$  (Eq. 17). Therefore, our method can be applied to weakly coupled oscillators in general.

One advantage of the proposed method is that it is applicable to oscillators in a synchronous state. It is noted that when estimating the coupling function  $q(\phi_i, \phi_j)$ , the oscillators must be in a completely asynchronous state [25, 26]. Moreover, it has been demonstrated that synchronization between oscillators deteriorates the inference accuracy of the averaged joint function  $\gamma(\phi_i - \phi_j)$  [35, 56]. Recently, it has been reported that methods based on machine learning (reservoir computing) do not provide good estimation accuracy when the oscillators are synchronized [57]. In contrast,

the proposed method can accurately estimate the coupling strength even when the oscillators are well-synchronized (Figs. 2, 3, and 4). The proposed method can accurately infer the network even when the Brusselator oscillators and clock cell models are strongly synchronized in the network.

The proposed method is based on three assumptions, (i) the coupling is uniform, (ii) the coupling function is a sinusoidal function, and (iii) the observed oscillatory signal is smooth and close to the sinusoidal function. First, the assumption (i) is valid for systems in which the coupling mechanism between elements is the same, including some systems of cardiac cells [40] and neurons [7, 41, 42]. Second, the assumption (ii) was shown to be valid in the vicinity of the Hopf bifurcation. In this study, it has been shown that the proposed method can accurately infer the network structure even for the Brusselator oscillator system not very close to the Hopf bifurcation point, as illustrated in Figs. 3 (c) and (d). This result indicates that the proposed method is effective even if assumption (ii) is not satisfied. As an extended model, we may also consider a coupling function of the form  $\gamma(\phi_i - \phi_j) = \sum_{k=1}^M a_k \cos(\phi_i - \phi_j) + b_k \sin(\phi_i - \phi_j)$  [29, 34, 58]. However, it is important to note that it would not be possible to infer the higher harmonic component when oscillators are strongly synchronized. This is because the data only provides information on the coupling function in the vicinity of the synchronized state ( $\phi_i - \phi_j \approx \text{const}$ ), which implies that the high-frequency model is considered to have no practical identifiability [59]. To infer the higher harmonic component, it is necessary to stimulate the system to desynchronize. In addition, an important future step to further improve the performance is to incorporate the variable selection into the proposed method. This could be achieved by using the sparse regression [60, 61] or the likelihood ratio test [62]. Finally, the assumption (iii) is necessary to reconstruct the phase using the Hilbert transform. Here, we used the Hilbert transform, which is one of the most commonly used methods for reconstructing the phase from oscillatory signals. Our results demonstrate that the proposed method can accurately infer the network even when the waveform deviates from the sinusoidal function. The proposed method is also applicable to phases reconstructed by methods other than the Hilbert transform. For example, when the waveform is distorted, we may use the protophase to phase transform [30] or the extended Hilbert transform [46, 48]. Similarly, for systems exhibiting marker events such as neural spikes, we may use linear interpolation for phase reconstruction [63, 64]. One avenue for future research is to apply of the proposed method to a range of phenomena described above, and infer the coupling network between oscillators.

In this study, we have proposed a method for inferring the coupling network from time series data measured from oscillators. The network inferred here is the coupling between oscillators in a reduced phase oscillator model. The inferred coupling network will provide important insights into the synchronization mechanism of oscillators. Moreover, unlike correlations between time series, this network captures causal relationships. Therefore, this network, which represents one of the forms of effective connectivity in the field of neuroscience [65, 66], is expected to provide important insights into the information flow in the brain. Consequently, the application of the proposed method to oscillatory signals obtained from various systems (e.g., SCN [67] and spinal cord [68]) would offer valuable insights into the mechanisms of synchronization and information flow in the brain. Furthermore, the potential diagnostic markers of brain disease could be identified by inferring the network from multi-electrode EEG and fMRI data [69–71].

## ACKNOWLEDGEMENT

We thank Arkady Pikovsky and Michael Rosenblum for helpful discussions. This study was supported by JSPS KAKENHI (Nos. JP23K19987 and JP24K20853) and AMED-CREST (No. JP23gm1710004h0002) to A.M., JSPS KAKENHI (Nos. JP21K12056, JP22K18384, and JP23K27487) to H.K., JSPS KAKENHI (Nos. JP18K11560, JP21H03559, JP21H04571, JP22H03695, and JP23K24950) and AMED (Nos. JP21wm0525004 and JP223fa627001) to R.K.

### Appendix A: Derivation of the phase equation

We derive the phase equation (3) from the dynamical equation (4) of the weakly coupled oscillators. The time derivative of the phase  $\phi_i = \Phi(\mathbf{X}_i)$  ( $i = 1, 2, \dots, N$ ) can be written as

$$\frac{d\phi_i}{dt} = \text{grad}_{\mathbf{X}}\Phi|_{\mathbf{X}=\mathbf{X}_i(t)} \cdot \frac{d\mathbf{X}_i}{dt} = \text{grad}_{\mathbf{X}}\Phi|_{\mathbf{X}=\mathbf{X}_i(t)} \cdot \left( \mathbf{F}_i(\mathbf{X}_i) + \epsilon \sum_{j=1}^N \mathbf{Q}_{ij}(\mathbf{X}_i, \mathbf{X}_j) + \epsilon \boldsymbol{\eta}_i(t) \right) \quad (\text{A1})$$

$$= \omega + \text{grad}_{\mathbf{X}}\Phi|_{\mathbf{X}=\mathbf{X}_i(t)} \cdot \left( \epsilon \mathbf{f}_i(\mathbf{X}_i) + \epsilon \sum_{j=1}^N \mathbf{Q}_{ij}(\mathbf{X}_i, \mathbf{X}_j) + \epsilon \boldsymbol{\eta}_i(t) \right). \quad (\text{A2})$$

In the derivation of Eq. (A2) from Eq. (A1), we used an expression that follows from the definition of the phase function:

$$\text{grad}_{\mathbf{X}}\Phi \cdot \bar{\mathbf{F}}(\mathbf{X}) = \omega. \quad (\text{A3})$$

Suppose that the perturbations are small and the orbit  $\mathbf{X}(t)$  stays in the vicinity of the limit-cycle orbit  $\mathbf{X}_0(t)$ , i.e.,  $\|\mathbf{X}(t) - \mathbf{X}_0(t)\| = O(\epsilon)$ , we can derive the phase equation

$$\frac{d\phi_i}{dt} = \omega + \mathbf{Z}(\phi_i) \cdot \left( \epsilon \mathbf{f}_i(\mathbf{X}_0(\phi_i)) + \epsilon \sum_{j=1}^N \mathbf{Q}_{ij}(\mathbf{X}_0(\phi_i), \mathbf{X}_0(\phi_j)) + \epsilon \boldsymbol{\eta}_i(t) \right) + O(\epsilon^2), \quad (\text{A4})$$

where  $\mathbf{Z}(\phi) := \text{grad}_{\mathbf{X}}\Phi|_{\mathbf{X}=\mathbf{X}_0(\phi/\omega)}$  is the phase sensitivity function. Finally, we can derive the phase equation (4) from Eq.(A4) by introducing following functions:  $\nu_i(\phi_i) := \mathbf{Z}(\phi_i) \cdot \mathbf{f}_i(\mathbf{X}_0(\phi_i))$  and  $q_{ij}(\phi_i, \phi_j) := \mathbf{Z}(\phi_i) \cdot \mathbf{Q}_{ij}(\mathbf{X}_0(\phi_i), \mathbf{X}_0(\phi_j))$ .

### Appendix B: Details of the naive method for inferring the oscillator network

In this Appendix, we describe the details of the naive method (Sec. III). The naive method consists of two steps: (i) phase reconstruction by the Hilbert transform and (ii) parameter estimation by maximizing the likelihood function.

#### 1. Phase reconstruction by the Hilbert transform

The Hilbert Transform is a widely used method to reconstruct the phase from the observed signal  $y(t)$  [45]. First, we preprocess the signal to mitigate the Gibbs phenomenon [46]: we extract the peaks from the signal and restrict the analysis from the first peak to the last peak. Then we reconstruct the phase using the following formula

$$\hat{\phi}_k := \arg(y_k + iH_d[y_k]), \quad (\text{B1})$$

where  $\hat{\phi}_k$  is the reconstructed phase at time  $t = kh$ ,  $\arg(z)$  is the argument of a complex number  $z$ ,  $H_d[y_k]$  is the discrete Hilbert transform [46, 72] of the signal  $\{y_k\}$  ( $k = 0, 1, \dots, K-1$ ). Note that the signal  $y_k = y(kh)$  is observed at  $N$  time steps with a constant interval  $h$ .

## 2. Parameter estimation by maximizing the likelihood function

The Naive method assumes that the data are generated from the averaged phase equation (12) and estimates the parameters using the maximum likelihood method. The log-likelihood function that corresponds to Eq. (12) can be written as follows [32, 34, 73].

$$l(\alpha, \boldsymbol{\theta}_1, \boldsymbol{\theta}_2, \dots, \boldsymbol{\theta}_N) = \sum_{i=1}^N l_i(\alpha, \boldsymbol{\theta}_i), \quad (\text{B2})$$

$$l_i(\alpha, \boldsymbol{\theta}_i) = -\frac{K}{2} \log(2\pi h s_i^2) - \frac{1}{2h s_i^2} \sum_{k=0}^{K-1} \left[ \delta \hat{\phi}_{i,k} - h \left\{ \omega_i + \sum_{j=1}^N c_{ij} \sin(\hat{\phi}_{j,k} - \hat{\phi}_{i,k} + \alpha) \right\} \right]^2, \quad (\text{B3})$$

where,  $\boldsymbol{\theta}_i := (\omega_i, c_{i1}, c_{i2}, \dots, c_{iN}, \sigma_i)$  is the vector of parameters of the  $i$ -th oscillator,  $\hat{\phi}_{i,k}$  is the reconstructed phase of the  $i$ -th oscillator at time  $t = kh$ , and  $\delta \hat{\phi}_{i,k} := \hat{\phi}_{i,k+1} - \hat{\phi}_{i,k}$  is its time difference.

In the maximum likelihood method, the parameters  $\boldsymbol{\theta}$  are obtained by maximizing the log likelihood  $l(\boldsymbol{\theta})$ . Unfortunately, it is difficult to find the parameter that maximizes  $l(\boldsymbol{\theta})$  in this case because the log-likelihood function  $l(\boldsymbol{\theta})$  is a nonlinear function of the parameter  $\alpha$ . However, assuming  $\alpha$  is known, the function  $l_i(\alpha, \boldsymbol{\theta}_i)$  is a quadratic function of the parameters  $\boldsymbol{\theta}_i$  and it is easy to maximize  $l_i(\alpha, \boldsymbol{\theta}_i)$

$$\hat{\boldsymbol{\theta}}_i(\alpha) = \arg \max_{\boldsymbol{\theta}_i} l_i(\alpha, \boldsymbol{\theta}_i). \quad (\text{B4})$$

Note that the log likelihood is a function of a single variable  $\alpha$  because it is the sum of the functions  $l_i(\alpha, \hat{\boldsymbol{\theta}}_i(\alpha))$

$$l(\alpha) := \sum_{i=1}^N l_i(\alpha, \hat{\boldsymbol{\theta}}_i(\alpha)) \quad (\text{B5})$$

Thus, the maximum likelihood estimator  $\{\hat{\alpha}, \hat{\boldsymbol{\theta}}_i(\hat{\alpha})\}$  ( $i = 1, 2, \dots, N$ ) can be calculated by finding  $\alpha$  that maximizes the log-likelihood  $l(\alpha)$  using the Brent method [49] within a range of  $-\pi/2 < \alpha \leq \pi/2$  and substituting  $\hat{\alpha}$  to Eq.(B4). The parameter estimation procedure is summarized as follows:

- (i) Find  $\alpha = \hat{\alpha}$  that maximizes the log-likelihood  $l(\alpha)$  (Eq. B5) using the Brent method within a range of  $-\pi/2 < \alpha \leq \pi/2$ .
- (ii) Obtain the maximum likelihood estimate of the parameters  $\{\hat{\boldsymbol{\theta}}_i\}$  ( $i = 1, 2, \dots, N$ ) by substituting  $\alpha = \hat{\alpha}$  into Eq. (B4).

### Appendix C: Averaging approximation of the stochastic Winfree model

We show that the stochastic Winfree model (Eqs.13 and 14) is reduced to Eq. (12) by the averaging approximation. To avoid confusion, we rewrite the stochastic Winfree model (Eqs.13 and 14) as

$$\frac{d\phi_1}{dt} = \tilde{\omega}_1 - 2\tilde{c} \sin \phi_1 (1 + \cos \phi_2) + \tilde{\sigma}_1 \sin \phi_1 \xi_1(t), \quad (\text{C1})$$

$$\frac{d\phi_2}{dt} = \tilde{\omega}_2 - 2\tilde{c} \sin \phi_2 (1 + \cos \phi_1) + \tilde{\sigma}_2 \sin \phi_2 \xi_2(t), \quad (\text{C2})$$

This is a non-averaged model Eq.(4) with

$$\omega + \epsilon \nu_i(\phi_i) = \tilde{\omega}_i, \quad (\text{C3})$$

$$\epsilon q_{ij}(\phi_i, \phi_j) = \begin{cases} -2\tilde{c} \sin \phi_i (1 + \cos \phi_j) & (i \neq j) \\ 0 & (i = j) \end{cases} \quad (\text{C4})$$

$$Z(\phi_i) = \sin \phi_i, \quad (\text{C5})$$

$$\eta_i(t) = \tilde{\sigma}_i \xi_i(t), \quad (\text{C6})$$

$$v_i = \tilde{\sigma}_i, \quad (\text{C7})$$



where the phase sensitivity function  $\mathbf{Z}(\phi_i)$  and the noise vector  $\boldsymbol{\eta}_i(t)$  are assumed to be scalars and are denoted by  $Z(\phi_i)$  and  $\eta_i(t)$ , respectively. We calculate the averaged frequency  $\omega_i$ , coupling strength  $c_{ij}$ , coupling function  $\gamma_{ij}$ , and noise  $\sigma_i$ . By substituting Eq.(C3) into Eq.(6), we have the averaged frequency

$$\omega_i = \tilde{\omega}_i. \quad (\text{C8})$$

For  $i \neq j$ , we have

$$\begin{aligned} \int_0^{2\pi} q_{ij}(\psi, \psi + \phi) d\psi &= \int_0^{2\pi} -\frac{2\tilde{c}}{\epsilon} \sin \psi (1 + \cos(\psi + \phi)) d\psi \\ &= \frac{\tilde{c}}{\epsilon} \int_0^{2\pi} \{-2 \sin \psi - \sin(\phi + 2\psi) + \sin \phi\} d\psi \\ &= \frac{2\pi\tilde{c}}{\epsilon} \sin \phi. \end{aligned} \quad (\text{C9})$$

Substituting this into Eqs. (7) and (8), we obtain the averaged coupling strength and the averaged coupling function,

$$c_{ij} = \frac{\epsilon}{\sqrt{\pi}} \left\| \frac{1}{2\pi} \int_0^{2\pi} q_{ij}(\psi, \psi + \phi) d\psi \right\| = \frac{\epsilon}{\sqrt{\pi}} \left\| \frac{\tilde{c}}{\epsilon} \sin \phi \right\| = \tilde{c}, \quad (\text{C10})$$

$$\gamma_{ij}(\phi) = \sqrt{\pi} \frac{\int_0^{2\pi} q_{ij}(\psi, \psi + \phi) d\psi}{\left\| \int_0^{2\pi} q_{ij}(\psi, \psi + \phi) d\psi \right\|} = \sqrt{\pi} \frac{\frac{2\pi\tilde{c}}{\epsilon} \sin \phi}{\left\| \frac{2\pi\tilde{c}}{\epsilon} \sin \phi \right\|} = \sin \phi, \quad (\text{C11})$$

respectively. We obtain the variance of the averaged noise by substituting Eq.(C5) into Eq. (9)

$$\sigma_i^2 = \frac{v_i^2}{2\pi} \int_0^{2\pi} \mathbf{Z}^T(\phi) \mathbf{Z}(\phi) d\phi = \frac{\tilde{\sigma}_i^2}{2\pi} \int_0^{2\pi} \sin^2 \phi d\phi = \frac{\tilde{\sigma}_i^2}{2}. \quad (\text{C12})$$

Substituting Eqs.(C10)–(C12) into Eq. (4), we have the averaged equation.

$$\frac{d\phi_1}{dt} = \tilde{\omega}_1 + \tilde{c} \sin(\phi_2 - \phi_1) + \frac{\tilde{\sigma}_1}{\sqrt{2}} \xi_1(t), \quad (\text{C13})$$

$$\frac{d\phi_2}{dt} = \tilde{\omega}_2 + \tilde{c} \sin(\phi_1 - \phi_2) + \frac{\tilde{\sigma}_2}{\sqrt{2}} \xi_2(t). \quad (\text{C14})$$

The discretized version of Eqs.(C13) and (C14) is the model used in the inference Eq. (12) with  $c_{11} = c_{22} = 0$ ,  $c_{12} = c_{21} = \tilde{c}$ ,  $\sigma_i = \tilde{\sigma}_i/\sqrt{2}$ , and  $\alpha = 0$ .

#### Appendix D: Derivation of the circle map

We derive the circle map (17) from the non-averaged phase equation (4). Although in Eq. (4), the Stratonovich interpretation is usually employed in the literature [5, 7], we employ the Ito interpretation for convenience. This treatment does not yield any significant error because the difference between these interpretations is of  $O(v_i^2)$ , where  $v_i^2$  is the noise strength, and we are assuming  $v_i^2 \ll \epsilon$  in the present paper. With the Ito interpretation,  $\phi_i(t)$  and  $\boldsymbol{\eta}_i(t)$  are not correlated.

First note that the relative phase  $\psi_i(t) = \phi_i(t) - \omega t$  is a slow variable because  $\dot{\phi}_i = \omega + O(\epsilon)$  in Eq. (4). Thus, we have

$$\psi_i(s) = \psi_i(t) + O(\epsilon) \quad \text{for } t < s < t + T. \quad (\text{D1})$$

Integrate both sides of Eq. (4) from  $t$  to  $t + T$  and using Eq. (D1), we obtain

$$\begin{aligned}
\Delta\phi_i(t) &= \phi_i(t+T) - \phi_i(t) \\
&= T\omega + \int_t^{t+T} \left\{ \epsilon\nu_i(\phi_i(s)) + \epsilon \sum_{j=1}^N g_{ij}(\phi_i(s), \phi_j(s)) + \mathbf{Z}(\phi_i(s)) \cdot \boldsymbol{\eta}_i(s) \right\} ds, \\
&= T\omega + \int_t^{t+T} \left\{ \epsilon\nu_i(\omega s + \psi_i(s)) + \epsilon \sum_{j=1}^N g_{ij}(\omega s + \psi_i(s), \omega s + \psi_j(s)) + \mathbf{Z}(\omega s + \psi_i(s)) \cdot \boldsymbol{\eta}_i(s) \right\} ds \\
&= T\omega + \int_t^{t+T} \left\{ \epsilon\nu_i(\omega s + \psi_i(t)) + \epsilon \sum_{j=1}^N g_{ij}(\omega s + \psi_i(t), \omega s + \psi_j(t)) + \mathbf{Z}(\omega s + \psi_i(t)) \cdot \boldsymbol{\eta}_i(s) \right\} ds + O(\epsilon^2, \epsilon v_i^2), \\
&= T\omega_i + T \sum_{j=1}^N c_{ij} \gamma_{ij} (\phi_j(t) - \phi_i(t)) + \tilde{\eta}_i(t) + O(\epsilon^2, \epsilon v_i^2), \tag{D2}
\end{aligned}$$

where  $\omega_i$ ,  $c_{ij}$  and  $\gamma_{ij}$  are defined in Eqs. (6)–(8), respectively. The noise term is given by

$$\tilde{\eta}_i(t) := \int_t^{t+T} \mathbf{Z}(\omega s + \psi_i(t)) \cdot \boldsymbol{\eta}_i(s) ds, \tag{D3}$$

which is Gaussian because  $\tilde{\eta}_i$  is a weighted sum of independent Gaussian noise. The mean and the variance of  $\tilde{\eta}_i(t)$  are given as

$$\mathbb{E}[\tilde{\eta}_i(t)] = \mathbb{E} \left[ \int_t^{t+T} \mathbf{Z}(\omega s + \psi_i(t)) \cdot \boldsymbol{\eta}_i(s) ds \right] = \int_t^{t+T} \mathbf{Z}(\omega s + \psi_i(t)) \cdot \mathbb{E}[\boldsymbol{\eta}_i(s)] ds = 0, \tag{D4}$$

$$\begin{aligned}
\text{Cov}[\tilde{\eta}_i(t), \tilde{\eta}_j(t+mT)] &= \mathbb{E} \left[ \int_t^{t+T} \mathbf{Z}(\omega s + \psi_i(t)) \cdot \boldsymbol{\eta}_i(s) ds \int_{t+mT}^{t+(m+1)T} \mathbf{Z}(\omega s' + \psi_j(t+mT)) \cdot \boldsymbol{\eta}_j(s') ds' \right] \\
&= \mathbb{E} \left[ \int_t^{t+T} ds \int_{t+mT}^{t+(m+1)T} ds' \mathbf{Z}^\top(\omega s + \psi_i(t)) \boldsymbol{\eta}_i(s) \boldsymbol{\eta}_j^\top(s') \mathbf{Z}(\omega s' + \psi_j(t+mT)) \right] \\
&= \int_t^{t+T} ds \int_{t+mT}^{t+(m+1)T} ds' \mathbf{Z}^\top(\omega s + \psi_i(t)) \mathbb{E}[\boldsymbol{\eta}_i(s) \boldsymbol{\eta}_j^\top(s')] \mathbf{Z}(\omega s' + \psi_j(t+mT)) \\
&= v_i^2 \delta_{ij} \delta_{m0} \int_t^{t+T} \mathbf{Z}^\top(\omega s + \psi_i(t)) \mathbf{Z}(\omega s + \psi_j(t+mT)) ds \\
&= T\sigma_i^2 \delta_{ij} \delta_{m0}, \tag{D5}
\end{aligned}$$

where  $m$  is an integer and  $\sigma_i$  is defined in Eq. (9). We denote  $\tilde{\eta}_i(mT)$  by  $\sqrt{T}\sigma_i\xi_{i,m}$ , where  $\xi_{i,m}$  is an independent Gaussian random variable with  $E[\xi_{i,m}] = 0$  and  $E[\xi_{i,m}\xi_{j,n}] = \delta_{ij}\delta_{mn}$ . By neglecting the terms of  $O(\epsilon^2, \epsilon v_i^2)$ , we obtain the circle map given in Eq. (17).

- 
- [1] A. Pikovsky, M. Rosenblum, and J. Kurths, *Synchronization: A Universal Concept in Nonlinear Sciences*, Cambridge Nonlinear Science Series (Cambridge University Press, 2001).
- [2] A. T. Winfree, Biological rhythms and the behavior of populations of coupled oscillators, *Journal of theoretical biology* **16**, 15 (1967).
- [3] Y. Kuramoto, *Chemical Oscillations, Waves and Turbulence* (Springer, Berlin, 1984).
- [4] A. T. Winfree, *The geometry of biological time*, Vol. 12 (Springer Science & Business Media, 2001).
- [5] H. Nakao, Phase reduction approach to synchronisation of nonlinear oscillators, *Contemporary Physics* **57**, 188 (2016).
- [6] B. Ermentrout, Y. Park, and D. Wilson, Recent advances in coupled oscillator theory, *Philosophical Transactions of the Royal Society A* **377**, 20190092 (2019).
- [7] P. Ashwin, S. Coombes, and R. Nicks, Mathematical frameworks for oscillatory network dynamics in neuroscience, *The Journal of Mathematical Neuroscience* **6**, 1 (2016).

- [8] M. Barahona and L. M. Pecora, Synchronization in small-world systems, *Physical Review Letters* **89**, 054101 (2002).
- [9] T. Nishikawa, A. E. Motter, Y.-C. Lai, and F. C. Hoppensteadt, Heterogeneity in oscillator networks: Are smaller worlds easier to synchronize?, *Physical Review Letters* **91**, 014101 (2003).
- [10] Y. Kobayashi and H. Kori, Synchronization failure caused by interplay between noise and network heterogeneity, *Chaos: An Interdisciplinary Journal of Nonlinear Science* **26** (2016).
- [11] A. E. Motter, C. Zhou, and J. Kurths, Network synchronization, diffusion, and the paradox of heterogeneity, *Physical Review E* **71**, 016116 (2005).
- [12] M. Chavez, D.-U. Hwang, A. Amann, H. Hentschel, and S. Boccaletti, Synchronization is enhanced in weighted complex networks, *Physical Review Letters* **94**, 218701 (2005).
- [13] S. Boccaletti, V. Latora, Y. Moreno, M. Chavez, and D.-U. Hwang, Complex networks: Structure and dynamics, *Physics Reports* **424**, 175 (2006).
- [14] A. Arenas, A. Díaz-Guilera, J. Kurths, Y. Moreno, and C. Zhou, Synchronization in complex networks, *Physics Reports* **469**, 93 (2008).
- [15] T. Ichinomiya, Frequency synchronization in a random oscillator network, *Physical Review E* **70**, 026116 (2004).
- [16] J. G. Restrepo, E. Ott, and B. R. Hunt, Onset of synchronization in large networks of coupled oscillators, *Physical Review E* **71**, 036151 (2005).
- [17] J. Gómez-Gardenes, S. Gómez, A. Arenas, and Y. Moreno, Explosive synchronization transitions in scale-free networks, *Physical Review Letters* **106**, 128701 (2011).
- [18] F. A. Rodrigues, T. K. D. Peron, P. Ji, and J. Kurths, The Kuramoto model in complex networks, *Physics Reports* **610**, 1 (2016).
- [19] O. V. Popovych and P. A. Tass, Control of abnormal synchronization in neurological disorders, *Frontiers in Neurology* **5**, 268 (2014).
- [20] M. Asllani, P. Expert, and T. Carletti, A minimally invasive neurostimulation method for controlling abnormal synchronisation in the neuronal activity, *PLoS computational biology* **14**, e1006296 (2018).
- [21] Y.-Y. Liu, J.-J. Slotine, and A.-L. Barabási, Controllability of complex networks, *Nature* **473**, 167 (2011).
- [22] P. S. Skardal and A. Arenas, Control of coupled oscillator networks with application to microgrid technologies, *Science advances* **1**, e1500339 (2015).
- [23] M. Timme and J. Casadiego, Revealing networks from dynamics: an introduction, *Journal of Physics A: Mathematical and Theoretical* **47**, 343001 (2014).
- [24] T. Stankovski, T. Pereira, P. V. E. McClintock, and A. Stefanovska, Coupling functions: universal insights into dynamical interaction mechanisms, *Reviews of Modern Physics* **89**, 045001 (2017).
- [25] M. Rosenblum and A. Pikovsky, Inferring connectivity of an oscillatory network via the phase dynamics reconstruction, *Frontiers in Network Physiology* **3** (2023).
- [26] M. G. Rosenblum and A. S. Pikovsky, Detecting direction of coupling in interacting oscillators, *Physical Review E* **64**, 045202 (2001).
- [27] M. Paluš and A. Stefanovska, Direction of coupling from phases of interacting oscillators: An information-theoretic approach, *Physical Review E* **67**, 055201 (2003).
- [28] J. Miyazaki and S. Kinoshita, Determination of a coupling function in multicoupled oscillators, *Physical Review Letters* **96**, 194101 (2006).
- [29] I. T. Tokuda, S. Jain, I. Z. Kiss, and J. L. Hudson, Inferring phase equations from multivariate time series, *Physical Review Letters* **99**, 064101 (2007).
- [30] B. Kralemann, L. Cimponeriu, M. Rosenblum, A. Pikovsky, and R. Mrowka, Uncovering interaction of coupled oscillators from data, *Physical Review E* **76**, 055201 (2007).
- [31] B. Kralemann, A. Pikovsky, and M. Rosenblum, Reconstructing phase dynamics of oscillator networks, *Chaos: An Interdisciplinary Journal of Nonlinear Science* **21**, 025104 (2011).
- [32] T. Stankovski, A. Duggento, P. V. E. McClintock, and A. Stefanovska, Inference of time-evolving coupled dynamical systems in the presence of noise, *Physical Review Letters* **109**, 024101 (2012).
- [33] T. Stankovski, V. Ticcinielli, P. V. E. McClintock, and A. Stefanovska, Coupling functions in networks of oscillators, *New Journal of Physics* **17**, 035002 (2015).
- [34] K. Ota, I. Aihara, and T. Aoyagi, Interaction mechanisms quantified from dynamical features of frog choruses, *Royal Society Open Science* **7**, 191693 (2020).
- [35] I. T. Tokuda, Z. Levnajic, and K. Ishimura, A practical method for estimating coupling functions in complex dynamical systems, *Philosophical Transactions of the Royal Society A* **377**, 20190015 (2019).
- [36] K. Yoshimura and K. Arai, Phase reduction of stochastic limit cycle oscillators, *Physical Review Letters* **101**, 154101 (2008).
- [37] J.-n. Teramae, H. Nakao, and G. B. Ermentrout, Stochastic phase reduction for a general class of noisy limit cycle oscillators, *Physical Review Letters* **102**, 194102 (2009).
- [38] F. C. Hoppensteadt and E. M. Izhikevich, *Weakly connected neural networks* (Springer Science & Business Media, 1997).
- [39] H. Kori, Y. Kawamura, H. Nakao, K. Arai, and Y. Kuramoto, Collective-phase description of coupled oscillators with general network structure, *Physical Review E* **80**, 036207 (2009).
- [40] S. Alonso, M. Bär, and B. Echebarria, Nonlinear physics of electrical wave propagation in the heart: a review, *Reports on Progress in Physics* **79**, 096601 (2016).
- [41] C. Van Vreeswijk, L. Abbott, and G. Bard Ermentrout, When inhibition not excitation synchronizes neural firing, *Journal of Computational Neuroscience* **1**, 313 (1994).

- [42] T. Fujita, T. Fukai, and K. Kitano, Influences of membrane properties on phase response curve and synchronization stability in a model globus pallidus neuron, *Journal of Computational Neuroscience* **32**, 539 (2012).
- [43] H. Sakaguchi and Y. Kuramoto, A soluble active rotator model showing phase transitions via mutual entertainment, *Progress of Theoretical Physics* **76**, 576 (1986).
- [44] H. Kori, Y. Kuramoto, S. Jain, I. Z. Kiss, and J. L. Hudson, Clustering in globally coupled oscillators near a Hopf bifurcation: theory and experiments, *Physical Review E* **89**, 062906 (2014).
- [45] D. Gabor, Theory of communication. Part 3: Frequency compression and expansion, *Journal of the Institution of Electrical Engineers-part III: radio and communication engineering* **93**, 445 (1946).
- [46] A. Matsuki, H. Kori, and R. Kobayashi, An extended hilbert transform method for reconstructing the phase from an oscillatory signal, *Scientific Reports* **13**, 3535 (2023).
- [47] J. T. Ariaratnam and S. H. Strogatz, Phase diagram for the winfree model of coupled nonlinear oscillators, *Physical Review Letters* **86**, 4278 (2001).
- [48] E. Gengel and A. Pikovsky, Phase demodulation with iterative Hilbert transform embeddings, *Signal Processing* **165**, 115 (2019).
- [49] R. P. Brent, *Algorithms for minimization without derivatives* (Courier Corporation, 2013).
- [50] P. Glansdorff and I. Prigogine, *Thermodynamic theory of structure, stability and fluctuations structure, stability and fluctuations* (Wiley-Interscience, 1971).
- [51] J. A. Mohawk and J. S. Takahashi, Cell autonomy and synchrony of suprachiasmatic nucleus circadian oscillators, *Trends in Neurosciences* **34**, 349 (2011).
- [52] Q. Lu and J. Y. Kim, Mammalian circadian networks mediated by the suprachiasmatic nucleus, *The FEBS Journal* **289**, 6589 (2022).
- [53] J. C. Locke, P. O. Westermarck, A. Kramer, and H. Herzog, Global parameter search reveals design principles of the mammalian circadian clock, *BMC systems biology* **2**, 1 (2008).
- [54] H. Kori, Y. Kawamura, and N. Masuda, Structure of cell networks critically determines oscillation regularity, *Journal of theoretical biology* **297**, 61 (2012).
- [55] B. Kralemann, M. Frühwirth, A. Pikovsky, M. Rosenblum, T. Kenner, J. Schaefer, and M. Moser, In vivo cardiac phase response curve elucidates human respiratory heart rate variability, *Nature Communications* **4**, 1 (2013).
- [56] M. J. Panaggio, M.-V. Ciocanel, L. Lazarus, C. M. Topaz, and B. Xu, Model reconstruction from temporal data for coupled oscillator networks, *Chaos: An Interdisciplinary Journal of Nonlinear Science* **29** (2019).
- [57] A. Banerjee, J. D. Hart, R. Roy, and E. Ott, Machine learning link inference of noisy delay-coupled networks with optoelectronic experimental tests, *Physical Review X* **11**, 031014 (2021).
- [58] H. Daido, Order function and macroscopic mutual entrainment in uniformly coupled limit-cycle oscillators, *Progress of theoretical physics* **88**, 1213 (1992).
- [59] A. P. Browning, D. J. Warne, K. Burrage, R. E. Baker, and M. J. Simpson, Identifiability analysis for stochastic differential equation models in systems biology, *Journal of the Royal Society Interface* **17**, 20200652 (2020).
- [60] S. L. Brunton, J. L. Proctor, and J. N. Kutz, Discovering governing equations from data by sparse identification of nonlinear dynamical systems, *Proceedings of the national academy of sciences* **113**, 3932 (2016).
- [61] E. Nijholt, J. L. Ocampo-Espindola, D. Eroglu, I. Z. Kiss, and T. Pereira, Emergent hypernetworks in weakly coupled oscillators, *Nature communications* **13**, 4849 (2022).
- [62] R. Kobayashi, S. Kurita, A. Kurth, K. Kitano, K. Mizuseki, M. Diesmann, B. J. Richmond, and S. Shinomoto, Reconstructing neuronal circuitry from parallel spike trains, *Nature Communications* **10**, 1 (2019).
- [63] R. F. Galán, G. B. Ermentrout, and N. N. Urban, Efficient estimation of phase-resetting curves in real neurons and its significance for neural-network modeling, *Physical Review Letters* **94**, 158101 (2005).
- [64] K. Nakae, Y. Iba, Y. Tsubo, T. Fukai, and T. Aoyagi, Bayesian estimation of phase response curves, *Neural Networks* **23**, 752 (2010).
- [65] K. J. Friston, Functional and effective connectivity in neuroimaging: a synthesis, *Human Brain Mapping* **2**, 56 (1994).
- [66] R. Kobayashi and S. Shinomoto, Inference of monosynaptic connections from parallel spike trains: A review, *Neuroscience Research*, In press (2024).
- [67] J. Myung, S. Hong, D. DeWoskin, E. De Schutter, D. B. Forger, and T. Takumi, Gaba-mediated repulsive coupling between circadian clock neurons in the scn encodes seasonal time, *Proceedings of the National Academy of Sciences* **112**, E3920 (2015).
- [68] R. Kobayashi, H. Nishimaru, and H. Nishijo, Estimation of excitatory and inhibitory synaptic conductance variations in motoneurons during locomotor-like rhythmic activity, *Neuroscience* **335**, 72 (2016).
- [69] B. P. Rogers, V. L. Morgan, A. T. Newton, and J. C. Gore, Assessing functional connectivity in the human brain by fmri, *Magnetic resonance imaging* **25**, 1347 (2007).
- [70] T. Kawano, N. Hattori, Y. Uno, K. Kitajo, M. Hatakenaka, H. Yagura, H. Fujimoto, T. Yoshioka, M. Nagasako, H. Otomune, *et al.*, Large-scale phase synchrony reflects clinical status after stroke: An eeg study, *Neurorehabilitation and Neural Repair* **31**, 561 (2017).
- [71] M. P. van den Heuvel and O. Sporns, A cross-disorder connectome landscape of brain dysconnectivity, *Nat. Rev. Neurosci.* **20**, 435 (2019).
- [72] F. W. King, *Hilbert transforms*, *Encyclopedia of Mathematics and Its Applications*, 124, Vol. 1 (Cambridge University Press, 2009).
- [73] P. Lánský, Inference for the diffusion models of neuronal activity, *Mathematical Biosciences* **67**, 247 (1983).